Journal of Advanced Ceramics
2021, **10**(1): 98–107
https://doi.org/10.1007/s40145-020-0423-4
ISSN 2226-4108
CN 10-1154/TQ

Research Article

Enhanced dielectric, ferroelectric, and optical properties in rare earth elements doped PMN–PT thin films

Shun ZHOU[a], Dabin LIN[a,*], Yongming SU[a], Lin ZHANG[b,*], Weiguo LIU[a]

[a]*Thin Film and Optical Manufacturing Technology*, *Key Laboratory of Ministry of Education*, *Xi'an Technological University*, *Xi'an 710032*, *China*
[b]*Electronic Materials Research Laboratory*, *Key Laboratory of the Ministry of Education & International Center for Dielectric Research*, *School of Electronic Science and Engineering*, *Faculty of Electronic and Information Engineering*, *Xi'an Jiaotong University*, *Xi'an 710049*, *China*

Received: April 7, 2020; Revised: September 15, 2020; Accepted: September 15, 2020

Abstract: Rare earth (RE = La^{3+}, Sm^{3+}, Pr^{3+}) ion doped $Pb(Mg_{1/3}Nb_{2/3})O_3$–$PbTiO_3$ (RE–PMN–PT) ferroelectric thin films with compositions near the morphotropic phase boundary were grown on the $Pt/TiO_2/SiO_2/Si(100)$ substrate using sol–gel/spin coating method. The phase structure, electrical properties, and photoluminescence performance of thin films were investigated systematically. The highly (100)-preferred orientation was obtained in pure perovskite Sm–PMN–0.30PT thin films with an average grain size of 131 nm. After 2.5% Sm^{3+} doping, the PMN–0.30PT thin films exhibited a triple enhancement of dielectric permittivity with a maximum value of 3500 at 1 kHz, a low dielectric loss of 1.3%, and high remanent polarization of 17.5 μC/cm^2 at room temperature. In visible light and near-infrared band, the transmittance rate increased with PT content and showed the highest value of 85% in 2.5%Sm–PMN–0.31PT. In addition, the films presented strong red-orange emission at 599 nm, which was sensitively in temperature range of 248–273 K corresponding to the rhombohedral to monoclinic phase transition temperature.

Keywords: PMN–PT; rare earth doping; dielectric; ferroelectric; photoluminescence

1 Introduction

Multifunctional materials have attracted much attention owing to their excellent coupling functions such as electro-mechanical [1–3], electro-optical interaction [4,5], and electro-caloric effects [6], for various energy conversion and electronic applications. Recently, on purpose of the combination of piezoelectric (electro-mechanical) and photoluminescence (electro-optical) effects, photoluminescence (PL) characteristics of rare earth (RE) ion doped ferroelectric materials were extensively investigated [5,7–10]. Because of the rich ion energy level and 4f electronic transition characteristics of rare earth elements, the RE ion doped piezoelectric materials have been considered to be good candidates for applications in the field of photonic devices [11,12], flat panel displays [13], and optical sensors [14].

$Pb(Mg_{1/3}Nb_{2/3})O_3$–$PbTiO_3$ (PMN–PT) ferroelectric crystals with compositions near the morphotropic phase boundary (MPB) have been widely investigated due to

* Corresponding authors.
E-mail: D. Lin, dabinlin@xatu.edu.cn;
L. Zhang, zhanglin.materials@gmail.com

their excellent dielectric ($\varepsilon_r > 6000$) and piezoelectric ($d_{33} > 2000$ pC/N) properties [15–18]. An ultrahigh piezoelectric coefficient ($d_{33} = 1500$ pC/N) was obtained in Sm^{3+} doped PMN–PT polycrystalline near MPB [1]. Because of the coupling function of excellent piezoelectric properties, efficient upconversion photoluminescence, and large electro-optic coefficient, RE (Pr^{3+}, Yb^{3+}, La^{3+}, Er^{3+}) doped PMN–PT based ceramic were intensively investigated [7,19–22].

For rare earth element doped ferroelectric thin films, a double enhanced dielectric permittivity was obtained in PMN–PT thin films through Pr^{3+} ion doping [23]. PMN–PT based thin films also possess many advantages of structure [24], electric and optic properties, such as high transmission [25], high optical damage threshold [20], low material toughness [26], and excellent chemical stability [27], making it as a potential candidate for photoluminescent matrix with RE ions and for optic device integration with powerful conditions. During the photoluminescence process, low energy photons were absorbed while high energy photons were produced. For example, the La^{3+} doped PMN–PT ceramics represented a high electro-optic (EO) coefficient on the value of 19.9×10^{-16} $(m/V)^{-2}$ [28,29], and a specific high optical transparency reaches up to 70% [19]. Therefore, the PMN–PT thin films doped with RE ions were expected to be multifunctional optical materials and deserved to be further investigated.

In this work, three RE ions (La^{3+}, Sm^{3+}, Pr^{3+}) were selected as activators in PMN–PT thin films. First, the RE–PMN–PT precursor solution was prepared by the sol–gel method and coated uniformly by spin coating method. Highly (100)-oriented RE–PMN–PT thin films were obtained after a gradient annealing processing. Second, the structure and electric properties of RE–PMN–PT thin films were measured. Third, the photoluminescence and transmittance spectra were tested at room temperature. Finally, the excitation and emission spectra were investigated at various energy levels and temperatures, respectively.

2 Material and methods

2. 1 Thin film preparation

First, the Ti metal layer of 100 nm in thickness was prepared by DC magnetron sputtering in Ar gas atmosphere [23]. To get pure (100)-oriented PMN–PT thin films, the Ti layer was annealed in a rapid thermal processing (RTP) furnace at 700 ℃ for 1 h. After that, a Pt layer with a thickness of 200 nm was deposited on the $TiO_2/SiO_2/Si$ (100) substrate.

Second, for sol–gel solution preparation, lead acetate trihydrate ($Pb(CH_3COO)_2\cdot3H_2O$), niobium ethoxide ($Nb(OC_2H_5)_5$), tetrabutyl titanate ($Ti(OC_4H_9)_4$), magnesium acetate tetrahydrate ($Mg(CH_3COO)_2\cdot4H_2O$), praseodymium acetyl acetonate ($C_{15}H_{21}PrO_6\cdot xH_2O$), samarium acetylacetonate ($C_{15}H_{21}SmO_6\cdot xH_2O$), and lanthanum acetylacetonate ($C_{15}H_{21}LaO_6\cdot xH_2O$) were employed as raw materials. 10 mol% more lead acetate trihydrate was added to reduce lead loss during heating processing and an excess of 5 mol% magnesium acetate tetrahydrate was added to promote perovskite phase production [30]. An organic solvent of ethylene glycol methyl ether ($C_3H_8O_2$) and acetylacetone($C_5H_8O_2$) was added to the precursor solution. The mixed solution was stirred for 4 h until the precursor solution was not precipitated. Then, the solution was made to volume again by a medium-pore filter paper, magnetically stirred for another half hour, and finally passed through a nylon microporous membrane with a pore size of 0.22 μm to obtain a stable solution of 0.35 mol/L. On the purpose of homogenization, the solution was left standing for 24–48 h.

Finally, the precursor solution was uniformly spin-coated on a $Pt/TiO_2/SiO_2/Si$ substrate by homogenization at 800 rpm for 10 s and subsequently sped up to 3000 rpm for 30 s. The sample was placed in a rapid thermal annealing furnace, undergoing a gradient annealing processing, including a preheating at 210 ℃ for 4 min to remove the organic solvent, a preheating at 400 ℃ for 5 min to remove organic matter, and a crystallization step at 630 ℃ for 3 min. Then, the high ratio perovskite phase 2.5%RE–PMN–xPT (x = 0.28–0.31) thin films were prepared. During the process, the changing annealing temperature and holding time would lead to perovskite phase degrading.

2. 2 Characterization

The phase structure and preferred orientation of 2.5%RE–PMN–xPT (x = 0.28–0.31) thin films were analyzed by X-ray diffraction (XRD) (Shimadzu X-6000, Kyoto, Japan) with a wide angle ($20°\leqslant2\theta\leqslant60°$) in steps of 0.02 at room temperature. The surface morphology of thin films was observed by field emission scanning electron microscope (FE-SEM) (Zeiss Gemini 500, Jena, Germany) and atomic force microscope (AFM) (Bruker Multimode 8, Billerica, MA, USA).

The dielectric properties were characterized by an impedance analyzer (HP4284, Hewlett Packard, CA, USA) with a precision LCR meter connected to a heating/cooling stage (THMSE 600, Linkam, UK). The ferroelectric hysteresis loops and leakage current density were measured using a standard ferroelectric system (TF-2000, aixACCT, Germany). The *P*–*E* loops were measured at 1 kHz. To investigate the transmittance, thin films were deposited on a quartz plate with a diameter of 15 mm and measured using a spectrophotometer (U3501, Hitachi, Japan) in a wavelength range of 200–1200 nm. The photoluminescence properties of thin films were tested at room temperature using a steady-state fluorescence spectrometer (FLS980, Edinburgh, UK) with a liquid nitrogen temperature control system and PL spectra were recorded at different excitation energies.

3 Results and discussion

3. 1 Structure and surface morphology

The XRD pattern of the A-site doped PMN–0.31PT thin films is shown in Fig. 1(a), including all samples deposited with different rare earth elements (Re = La^{3+}, Pr^{3+}, Sm^{3+}) on a Pt/TiO_2/SiO_2/Si substrate. The observed peaks at 2θ = 22.2°, 31.5°, 38.9°, 45.2°, 50.9°, 56.2°, are related to perovskite phase, corresponding to (100), (110), (111), (200), (220), (211), respectively. The pyrochlore phase at 2θ = 29.4° is clearly visible in Pr–PMN–0.31PT thin films. With annealing temperature increase to 630 ℃, the pyrochlore phase disappeared, which is caused by the low lead loss during annealing [23]. Figure 1(b) shows the XRD pattern of PMN–*x*PT thin films with Sm^{3+} dopant at different levels of PT. All samples exhibit a single perovskite phase structure, showing two strong peaks at 2θ = 22.2°, 45.2°, which indicates that (100) is the preferred growth direction for RE–PMN–0.31PT thin films.

Figures 1(c) and 1(d) show the percentage of (100)-orientation in RE–PMN–PT thin films. The preferential orientation parameter α_{hkl} calculated from the summation of the peaks from a given family of planes, is used to define the degree of preferred orientation [31,32]:

$$\alpha_{hkl} = \frac{I_{hkl}}{\sum I_{hkl}} \tag{1}$$

where I_{hkl} is the relative intensity of the corresponding diffraction peak. As shown in Fig. 1(d), the highest α_{hkl} value is found in 2.5%Sm–PMN–0.30PT thin films.

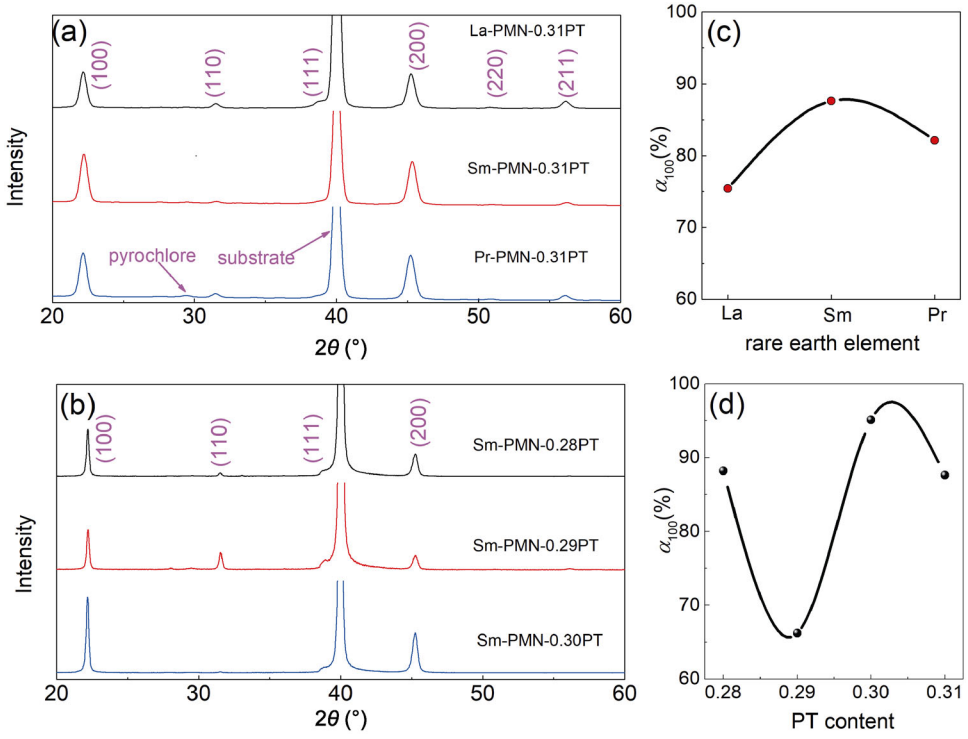

Fig. 1 XRD patterns of RE–PMN–PT (RE = La^{3+}, Sm^{3+}, Pr^{3+}) thin films: (a) and (b); the percentage of (100)-orientation in RE–PMN–PT (RE = La^{3+}, Sm^{3+}, Pr^{3+}) thin films: (c) and (d).

Figures 2(a)–2(c) show FE-SEM images of surface photomicrographs of RE–PMN–PT (RE = La^{3+}, Sm^{3+}, Pr^{3+}) thin films. The films possess a uniform, crack-free, and mirror-like surface structure. Figures 2(d)–2(f) show the grain size distribution in a region containing 400 grains, giving an average grain size of 133 nm, 131 nm, and 120 nm, respectively. Three-dimensional AFM images of RE–PMN–PT thin films in the scanning area of 2 μm × 2 μm are shown in Figs. 2(g)–2(i), representing the root square roughness (R_{rms}) is on order of 2.61 nm, 2.60 nm, and 2.49 nm, respectively.

3. 2 Dielectric properties

Temperature dependence of the dielectric permittivity and loss of La/Sm/Pr–PMN–0.31PT thin films at 1 kHz, 10 kHz, and 100 kHz are shown in Figs. 3(a)–3(c). The dielectric permittivity of La/Sm/Pr–PMN–0.31PT shows a frequency-dependent dispersion behavior in the temperature range from 25 to 150 ℃, exhibiting relaxor ferroelectric characteristics. There is no dielectric permittivity peak observed near 100 ℃, corresponding to T_{max} in the Sm^{3+} doped PMN–0.31PT ceramic of the same composition [1]. The dielectric loss of RE–PMN–0.31PT thin films is in range of 0.01–0.02 and does not exhibit obvious change at different measuring frequencies at room temperature, indicating that space charge has an extremely limited impact on dielectric properties. With temperature increase, a broad peak was observed at temperature in range of 80–100 ℃, which is close to T_{max} [1].

The relative dielectric permittivity ε_r as a function of rare-earth dopants at 25 ℃ is shown in Fig. 3(d). After doping, 50% double and triple enhancement of ε_r were observed, showing values of 1800, 2400, and 3500 in La^{3+}, Pr^{3+}, and Sm^{3+} doped PMN–0.31PT thin films at 1 kHz, respectively, which were attributed to its highly (100)-oriented texture. Owing to the MPB composition, a high permittivity is caused by the co-existence of rhombohedral and tetragonal phases, which can enhance the polarization isotropy and induce a low energy barrier for polarization rotation [33]. In addition, the substitution of RE would suppress Pb ion volatilization during the annealing process and inhibit the formation of intrinsic oxygen vacancies [34]. Thus, the improvement of dielectric permittivity can be partially ascribed to the effect of the reduction of defects and lattice distortion in RE–PMN–PT thin films. It is well known the dielectric permittivity of thin film is strongly

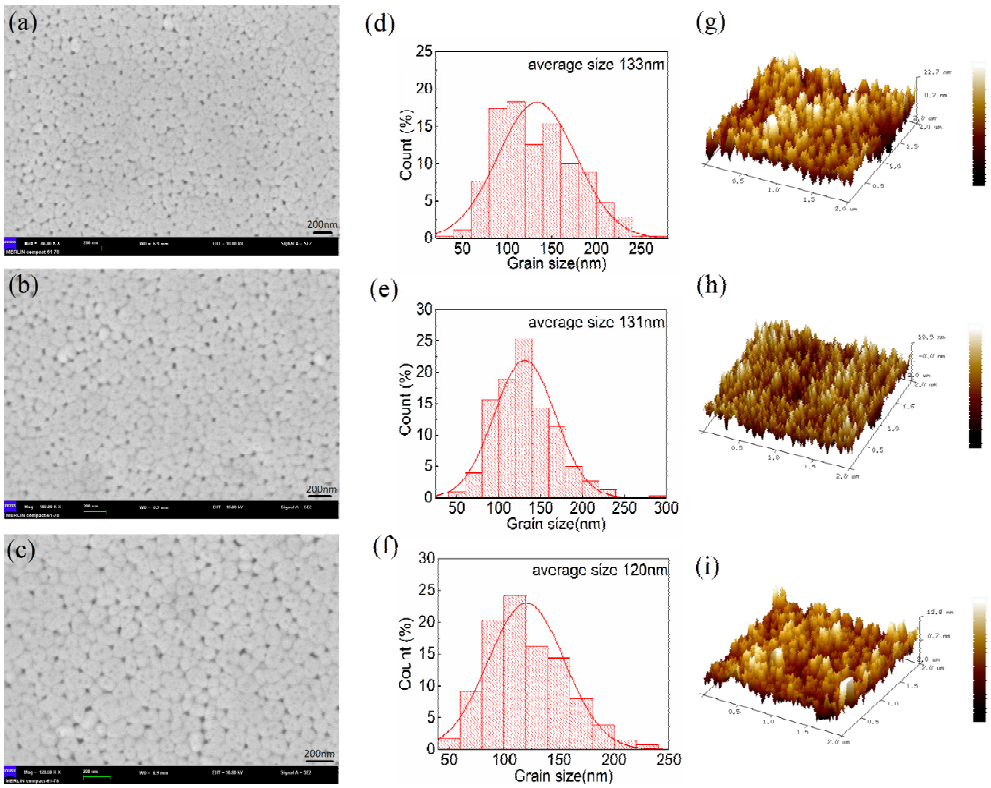

Fig. 2 Surface morphology of RE–PMN–PT (RE = La^{3+}, Sm^{3+}, Pr^{3+}) thin films: (a)–(c) SEM images, (d)–(f) grain size distributions, and (g)–(i) 3D AFM images, respectively.

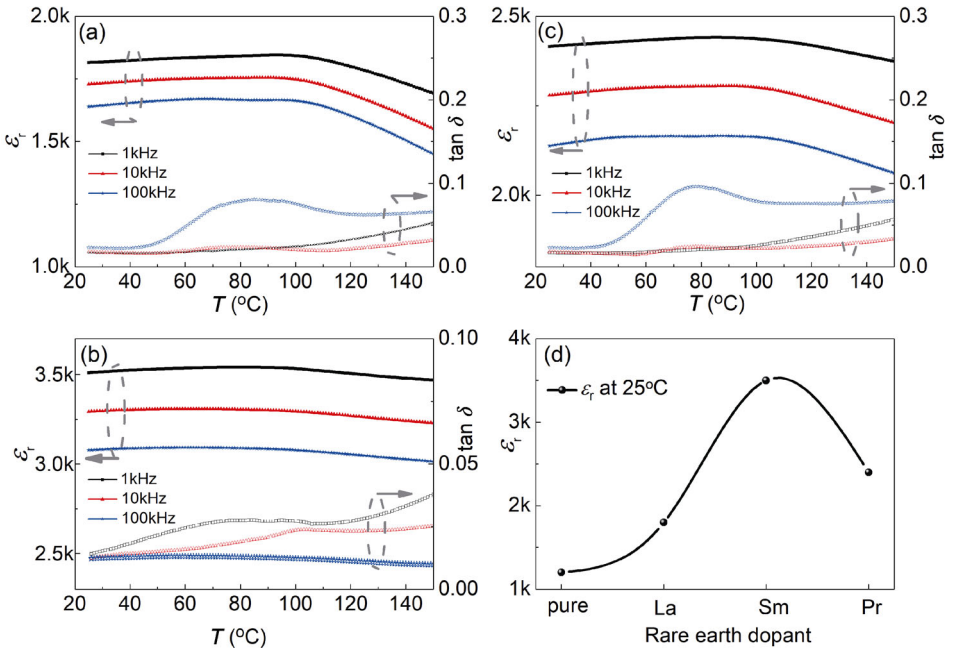

Fig. 3 Temperature dependence of dielectric permittivity and loss of RE–PMN–PT thin films: (a) La–PMN–0.31PT, (b) Sm–PMN–0.31PT, and (c) Pr–PMN–0.31PT; the comparison of dielectric permittivity between pure and RE–PMN–0.31PT thin films at 25 ℃.

affected by microstructure, substrates, and grain size. As shown in Fig. 2, the microstructures and grain size are similar in La^{3+}, Sm^{3+}, and Pr^{3+} doped PMN–PT thin films, respectively. The possible reason is the smaller ionic radius of Sm^{3+} (0.96) than that of La^{3+} (1.03) and Pr^{3+} (0.99) adverse to lattice distortion in PMN–PT thin films. Comparing with $NdScO_3$/$LaAlO_3$ crystal substrates [27,35], the Sm^{3+} doped PMN–0.30PT thin films also present higher dielectric permittivity, as shown in Table 1, giving a new way to prepare high-quality thin film on Pt substrate. The high permittivity and low dielectric loss make it suitable for capacitor applications.

3. 3 Ferroelectric properties

As shown in Fig. 4, the ferroelectric hysteresis loops (*P*–*E*) and leakage current density (*J*–*E*) of pure and RE–PMN–0.31PT were comparatively investigated. The largest remnant polarization P_r value of 17.5 μC/cm^2 was obtained in Sm^{3+} doped PMN–0.30PT thin films under an electric field of 400 kV/cm, as shown in Table 1. Comparing with pure PMN–PT thin films, the RE–PMN–PT thin films present higher remnant polarization (P_r) and lower leakage current. In ferroelectric thin films, defects such as oxygen vacancies near domain walls result in the domain wall pinning, which will lower the movement of domain walls, and eventually reduce remnant polarization (P_r) value and high leakage current density [34]. Furthermore, A-site vacancies will benefit the domain wall motion which will lead to the low coercive field and slanted *P*–*E* loops [36]. Therefore, enhancement of P_r values can be attributed to the increased domain wall mobility through doping [37]. Figure 4(b) shows the *J*–*E* curve of pure and RE doped PMN–0.31PT thin films. The leakage current

Table 1 Dielectric and ferroelectric properties in Sm^{3+} doped PMN–PT thin films at room temperature

Thin films	Substrates	Thickness (nm)	Method	ε_r@ 1 kHz	tanδ (%)	P_r (μC/cm^2)	Ref.
2.5%Sm–PMN–0.30PT	Pt/TiO_2/SiO_2/Si	450	Sol–gel	3500	1.3	17.5	This work
2.5%Pr–PMN–0.30PT	Pt/TiO_2/SiO_2/Si	450	Sol–gel	2400	1.5	17.3	[23]
PMN–0.30PT	Pt/TiO_2/SiO_2/Si	350	CSD	1710	0.8	—	[30]
PMN–0.32PT	$La_{0.5}Sr_{0.5}CoO_3$/$LaAlO_3$	150	PLD	~2500	~7	~11	[26]
Nb/La–PZT	Pt/Ti/SiO_2/Si	—	CSD	1350	2.5	26	[36]

ε_r dielectric permittivity; tanδ dielectric loss; P_r remanent polarization.

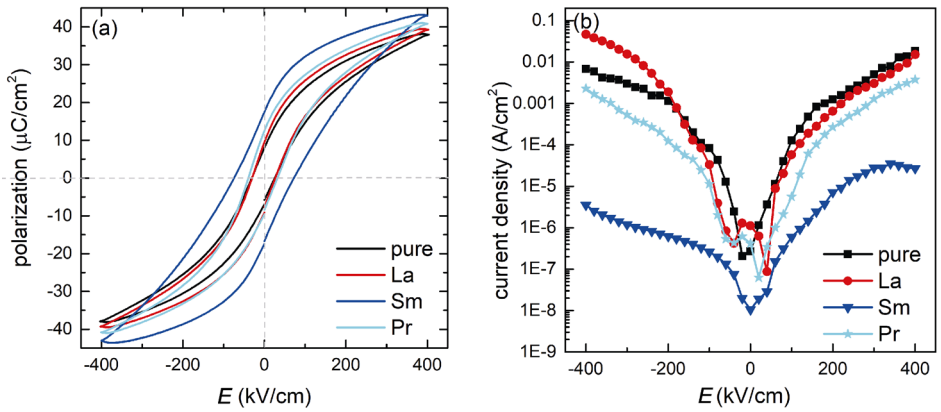

Fig. 4 (a) Ferroelectric hysteresis loops of RE–PMN–0.31PT (RE = La^{3+}, Sm^{3+}, Pr^{3+}) thin films; (b) leakage current density of RE–PMN0.31PT (RE = La^{3+}, Sm^{3+}, Pr^{3+}) thin films.

density is much lower in Sm^{3+} doped PMN–PT than that of pure PMN–PT thin films due to compensation of oxygen ion vacancy, coinciding with the low dielectric loss, as shown in Fig. 3(b).

3. 4 Photoluminescence properties

Based on the high dielectric and ferroelectric properties, the Pr^{3+} and Sm^{3+} doped PMN–PT thin films were selected to further investigation. Figures 5(a)–5(c) show photoluminescence excitation spectra and photoluminescence emission spectra of 2.5%RE–PMN–0.3PT thin films in the wavelength range of 300–550 nm and 550–675 nm, respectively. To discuss the excitation and emission processes, the energy level diagrams of RE ions are shown in Figs. 5(d) and 5(e).

The luminescence spectra and the emission mechanism of Pr^{3+}-doped perovskite materials have been investigated in many works, on the purpose of combined ferroelectric/piezoelectric and luminescence properties in lead-free piezoelectric crystals and thin films [38–41]. For PMN–PT thin films, the piezoelectric properties have been extensively reported [2,3,42,43]. As shown in

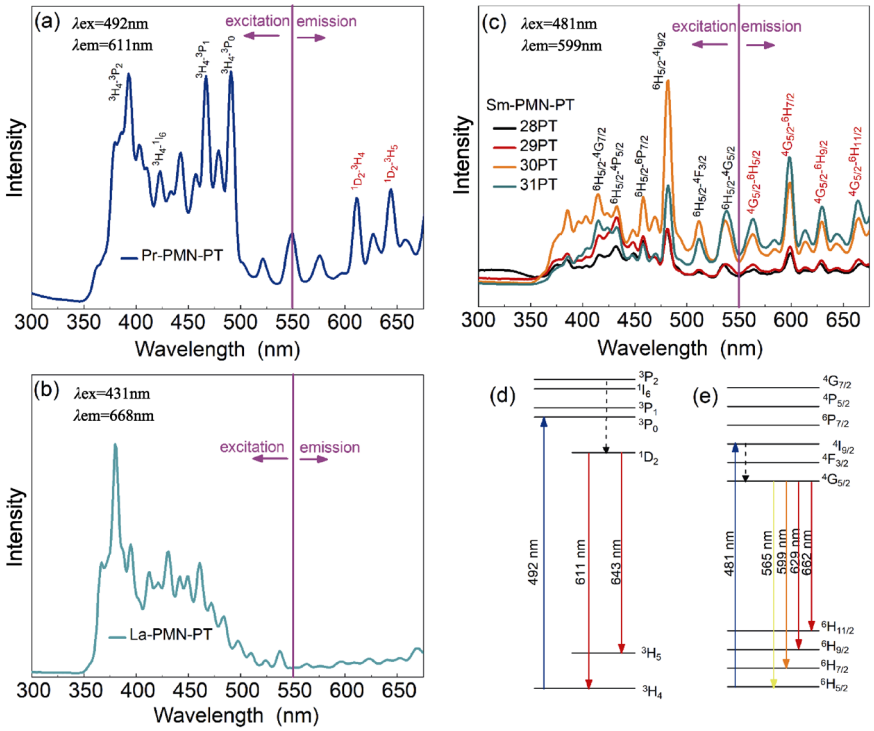

Fig. 5 Room temperature PL excitation spectra and emission spectra of RE–PMN–PT thin films: (a) Pr–PMN–0.31PT, (b) La–PMN–0.31PT, and (c) Sm–PMN–*x*PT (*x* = 0.28,0.29,0.30, 0.31); the energy level diagram of (d) Pr^{3+} and (e) Sm^{3+}.

Fig. 5(a), Pr-doped PMN–PT thin films exhibit a strong red-light emission characteristic and concentrate at 611 nm and 645 nm peaks under blue light excitation (440–505 nm). The spectrum consists of three strong absorption peaks at 397 nm, 468 nm, and 492 nm, which are mainly attributed to the $^3P_0$, $^3P_1$, and $^3P_2$ excited state of Pr^{3+} ion from the $^3H_4$ ground state to the typical f–f transition of Pr^{3+} ion. Similar to Pr^{3+} doped (Ca, Sr, Ba)TiO_3 [44] and NBT–STO [40] thin films excited by a UV light, there is a red emission at a wavelength of 611 nm, corresponding to the $^1D_2$–$^3H_4$ transition. The other red emission peak was observed at a wavelength of 643 nm belong to the $^1D_2$–$^3H_5$ transition.

As a comparison, the La–PMN–PT thin films were investigated, because there is no energy level in the 4f energy layer of La^{3+} ion. In previous work, La^{3+} ion can be used to improve the ferroelectric and dielectric properties in RE doped ferroelectric thin films with strong photoluminescence properties [45]. Figure 5(b) shows the excitation spectrum monitoring at 668 nm and emission spectrum excited at 431 nm. A strong excitation peak is detected at a wavelength of 380 nm and broad peaks are recorded in the wavelength range of 410–460 nm. For the emission spectra, there is no peak observed.

The effect of PT content on the photoluminescent excitation spectrum monitored at 599 nm emission and the emission spectrum excited at 481 nm is shown in Fig. 5(c). Six excitation peaks are observed in the wavelength range of 300–500 nm, corresponding to a typical f–f transition from the ground state $^6H_{5/2}$ to excited states $^4G_{7/2}$,$^4P_{5/2}$,$^6P_{7/2}$,$^4I_{9/2}$,$^4F_{3/2}$, and $^4G_{5/2}$, respectively. The maximum absorption is located at 482 nm. As PT content increases, the excitation intensity firstly increases, and reaches up to the maximum value at PT = 0.30, then decreases. On the other hand, a strong red-orange emission is observed at a wavelength of 599 nm ($^4G_{5/2}$–$^6H_{7/2}$) under blue light excitation at 481 nm, and other three emission peaks are found in the wavelength range of 550–730 nm, corresponding to 565 nm ($^4G_{5/2}$–$^6H_{5/2}$), 629 nm ($^4G_{5/2}$–$^6H_{9/2}$), and 662 nm ($^4G_{5/2}$–$^6H_{11/2}$). Obviously, the intensity of emission peaks presents a rising tendency as the increase of PT content in 0.25%Sm–PMN–xPT (x = 0.28–0.31) and reaches the maximum value when x = 0.31.

3. 5 Transparent spectra

Considering the potential application in photodetectors, the optic transmission of 0.25%Sm–PMN–xPT (x = 0.28, 0.29, 0.30, 0.31) thin films is measured in a wavelength range of 200–2000 nm, as shown in Fig. 6. Different from the RE–PZT and RE–PMN–PT ceramics [46,47], the absorbing is slight in the UV below 400 nm. It is interesting that the transmittance of 0.25%Sm–PMN–xPT thin films represents dependence on the PT content, which shows the highest value at x = 0.31. In wavelength range of 600–1200 nm, corresponding to red/orange light band and the near-infrared band, the transmittance rate is higher than 85% in 0.25%Sm–PMN–0.31PT thin films.

3. 6 Photoluminescence spectra at various powers and temperatures

To further understand the mechanism of photoluminescence of Sm^{3+} doped PMN–PT thin films, the photoluminescence spectra of 0.25%Sm–PMN–0.31PT thin films as a function of pump power and temperature are investigated, as shown in Fig. 7. Figure 7(a) shows photoluminescence excitation spectra and photoluminescence emission of 2.5%Sm–PMN–0.31PT thin films under the 599 nm emission and 481 nm excitation with various powers from 130 to 335 mW. The peak value of each emission band increased gradually with incident power. It is known that the photoluminescence intensity is related to the site symmetry change of RE^{3+} ions in the host materials [39,40]. There is a phase transition path of R–M–T–C in (100)-oriented PMN–PT crystal as temperature increases [48]. As shown in Fig. 7(b), the temperature dependent PL excitation spectrum and PL emission spectrum of 2.5%RE–PMN–0.31PT thin films under the 599 nm emission and 481 nm excitation are investigated at various temperatures in range of 248–398 K. An obvious increase in intensity of three peaks at 459, 513, and 543 nm can be observed

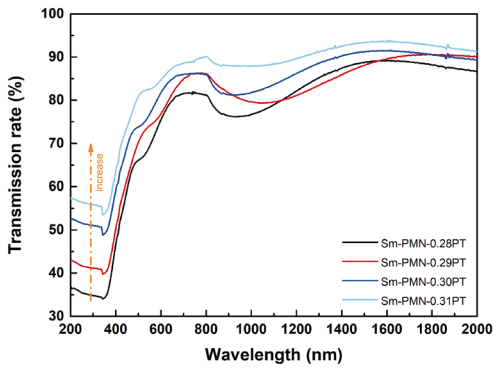

Fig. 6 Optical transmittance spectra of 2.5%Sm–PMN–xPT (x = 0.28, 0.29, 0.30, 0.31) thin films in the wavelength range of 200–1200 nm.

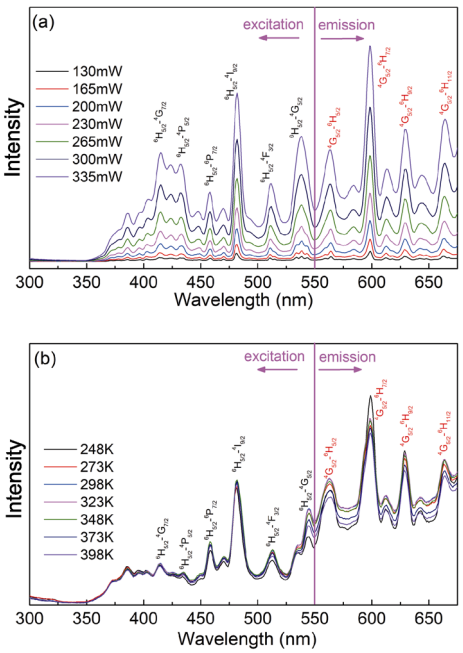

Fig. 7 PL excitation spectra and emission spectra of 2.5%Sm–PMN–0.31PT thin films: (a) at different energy levels in the range from 130 to 335 mW, (b) at a various temperature in the range of 248–398 K.

during temperature increase from 248 to 273 K, corresponding to rhombohedral to monoclinic phase transition temperature of host PMN–0.31PT [1]. On the other hand, a clear decrease in the red-orange emission is detected at 599 nm during the temperature increases from 248 to 273 K. In temperature range from 273 to 398 K, there is no clear change tendency in the excitation and emission spectrum, due to the mixed symmetry in Sm^{3+} ion-doped PMN–PT thin films with MPB compositions [1].

4 Conclusions

Highly (100)-oriented dense pure perovskite 2.5%RE–PMN–PT (RE = La^{3+}, Sm^{3+}, Pr^{3+}) thin films have been prepared by sol–gel/spin coating method. Dielectric properties were enhanced significantly in RE doped PMN–PT thin films. Especially, the dielectric permittivity reaches 3500 and 2400 at 1 kHz with dielectric loss of 1.3% and 1.5% in Sm^{3+} and Pr^{3+} doped PMN–PT thin films, respectively. Moreover, high remanent polarization of 17.5 μC/cm^2 and low leakage current density of 2.5×10^{-5} A/cm^2 at 400 kV/cm was obtained in the Sm^{3+} doped PMN–PT thin films. For optical properties, low absorption in the UV band below 400 nm, and high transmittance with value of 85% at wavelength in range of 600–1200 nm were found in Sm^{3+} doped PMN–PT thin films. A red emission at 611 nm and red-orange emission at 599 nm were observed in Pr^{3+} and Sm^{3+} doped PMN–0.31PT thin films, respectively, indicating the potential application in a multifunctional optoelectronic device.

Acknowledgements

We appreciate the funding from the National Natural Science Foundation of China (Nos. 51502232 and 51972263), National Basic Research Project (No. JCKY2016208A002), and Advanced Manufacturing Project (No. 41423020111).

References

[1] Li F, Lin D, Chen Z, *et al.* Ultrahigh piezoelectricity in ferroelectric ceramics by design. *Nat Mater* 2018, **17**: 349–354.

[2] Baek SH, Park J, Kim DM, *et al.* Giant piezoelectricity on Si for hyperactive MEMS. *Science* 2011, **334**: 958–961.

[3] Baek SH, Rzchowski MS, Aksyuk VA. Giant piezoelectricity in PMN-PT thin films: Beyond PZT. *MRS Bull* 2012, **37**: 1022–1029.

[4] Beechem TE, Goldflam MD, Sinclair MB, *et al.* Tunable infrared devices via ferroelectric domain reconfiguration. *Adv Opt Mater* 2018, **6**: 1800862.

[5] Chen XQ, Wang Q, Wu X, *et al*. Piezoelectric/photoluminescence effect in one-dimensional lead-free nanofibers. *Scripta Mater* 2018, **145**: 81–84.

[6] Feng ZY, Shi DQ, Zeng R, *et al*. Large electrocaloric effect of highly (100)-oriented $0.68PbMg_{1/3}Nb_{2/3}O_3$–$0.32PbTiO_3$ thin films with a $Pb(Zr_{0.3}Ti_{0.7})O_3/PbO_x$ buffer layer. *Thin Solid Films* 2011, **519**: 5433–5436.

[7] Lv Z, Qin YL, Zhang YC, *et al*. Efficient upconversion photoluminescence in transparent Pr^{3+}/Yb^{3+} co-doped $0.75Pb(Mg_{1/3}Nb_{2/3})O_3$–$0.25PbTiO_3$ ferroelectric ceramics. *Ceram Int* 2019, **45**: 10924–10929.

[8] Wang FF, Liu D, Chen ZB, *et al*. *In situ* reversible tuning of photoluminescence of an epitaxial thin film via piezoelectric strain induced by a $Pb(Mg_{1/3}Nb_{2/3})O_3$–$PbTiO_3$ single crystal. *J Mater Chem C* 2017, **5**: 9115–9120.

[9] Wu X, Lin J, Chen P, *et al.* Ho^{3+}-doped $(K,Na)NbO_3$-based multifunctional transparent ceramics with superior optical temperature sensing performance. *J Am Ceram Soc* 2019, **102**: 1249–1258.

[10] Du P, Luo LH, Li WP, *et al*. Upconversion emission in Er-doped and Er/Yb-codoped ferroelectric $Na_{0.5}Bi_{0.5}TiO_3$ and its temperature sensing application. *J Appl Phys* 2014, **116**: 014102.

[11] Wang ZL. Piezopotential gated nanowire devices: Piezotronics and piezo-phototronics. *Nano Today* 2010, **5**: 540–552.

[12] Paulish AG, Zagubisalo PS, Barakov VN, *et al*. Piezo-optical

transducer for high sensitive strain gauges. *IEEE Sensor J* 2018, **18**: 8318–8328.

[13] McDonald M. 39.3: Manufacture of flat panel displays using piezoelectric drop-on-demand ink jet. *SID Symposium Digest* 2003, **34**: 1186–1189.

[14] Tabib-Azar M, Garcia-Valenzuela A. Sensing means and sensor shells: A new method of comparative study of piezoelectric, piezoresistive, electrostatic, magnetic, and optical sensors. *Sensor Actuat A: Phys* 1995, **48**: 87–100.

[15] Zhang SJ, Li F. High performance ferroelectric relaxor-$PbTiO_3$ single crystals: Status and perspective. *J Appl Phys* 2012, **111**: 031301.

[16] Li F, Zhang S, Damjanovic D, *et al.* Local structural heterogeneity and electromechanical responses of ferroelectrics: Learning from relaxor ferroelectrics. *Adv Funct Mater* 2018, **28**: 1801504.

[17] Li Y, Tang Y, Chen J, *et al.* Enhanced pyroelectric properties and thermal stability of Mn-doped $0.29Pb(In_{1/2}Nb_{1/2})O_3$–$0.29Pb(Mg_{1/3}Nb_{2/3})O_3$–$0.42PbTiO_3$ single crystals. *Appl Phys Lett* 2018, **112**: 172901.

[18] Li SY, Sun EW, Tang LG, *et al*. Temperature dependence of full matrix material constants of [001]c poled $0.71Pb(Mg_{1/3}Nb_{2/3})O_3$–$0.29PbTiO_3$ single crystal. *J Appl Phys* 2018, **123**: 164102.

[19] Song ZZ, Zhang YC, Lu CJ, *et al*. Fabrication and ferroelectric/dielectric properties of La-doped PMN-PT ceramics with high optical transmittance. *Ceram Int* 2017, **43**: 3720–3725.

[20] Wei ZH, Huang YL, Tsuboi T, *et al*. Optical characteristics of Er^{3+}-doped PMN–PT transparent ceramics. *Ceram Int* 2012, **38**: 3397–3402.

[21] Wei Z, Tsuboi T, Nakai Y. The synthesis of Er^{3+}-doped PMN–PT transparent ceramic and its infrared luminescence. *Mater Lett* 2012, **68**: 57–59.

[22] Zeng JT, Wei ZH, Huang YL, *et al*. NIR to visible up-conversion luminescence of Er^{3+}-doped PMN-PT transparent ceramics. *J Am Ceram Soc* 2012, **95**: 2573–2578.

[23] Cai C, Zhang D, Liu W, *et al.* Synthesis, giant dielectric, and pyroelectric response of [001]-oriented Pr^{3+} doped $Pb(Mg_{1/3}Nb_{2/3})O_3$–$PbTiO_3$ ferroelectric nano-films grown on Si substrates. *Materials* 2018, **11**: 2392.

[24] Goel TC, Kumar P, James AR, *et al*. Processing and dielectric properties of sol-gel derived PMN-PT (68:32) thin films. *J Electroceram* 2004, **13**: 503–507.

[25] Li GR, Ruan W, Zeng JT, *et al*. The effect of domain structures on the transparency of PMN–PT transparent ceramics. *Opt Mater* 2013, **35**: 722–726.

[26] Pan JY, Men TL, Xu XY, *et al*. Domain growth dynamics in PMN-PT ferroelectric thin films. *J Mater Sci* 2019, **54**: 10600–10608.

[27] Wang J, Wong KH, Chan HLW, *et al*. Composition control and electrical properties of PMN-PT thin films around the morphotropic boundary. *Appl Phys A* 2004, **79**: 551–556.

[28] Ji WL, He XY, Zeng X, *et al*. Effects of PMN/PT ratio on optical and electro-optic properties of PLMNT transparent ceramics. *Ceram Int* 2015, **41**: 10387–10393.

[29] Ruan W, Li GR, Zeng JT, *et al*. Large electro-optic effect in La-doped $0.75Pb(Mg_{1/3}Nb_{2/3})O_3$–$0.25PbTiO_3$ transparent ceramic by two-stage sintering. *J Am Ceram Soc* 2010, **93**: 2128–2131.

[30] Keech R, Shetty S, Wang K, *et al*. Management of lead content for growth of {001}-oriented lead magnesium niobate-lead titanate thin films. *J Am Ceram Soc* 2016, **99**: 1144–1146.

[31] Brosnan KH, Messing GL, Meyer RJ, *et al*. Texture measurements in <001> fiber-oriented PMN-PT. *J Am Ceram Soc* 2006, **89**: 1965–1971.

[32] Lotgering FK. Topotactical reactions with ferrimagnetic oxides having hexagonal crystal structures—II. *J Inorg Nucl Chem* 1960, **16**: 100–108.

[33] Li F, Cabral MJ, Xu B, *et al.* Giant piezoelectricity of Sm-doped $Pb(Mg_{1/3}Nb_{2/3})O_3$–$PbTiO_3$ single crystals. *Science* 2019, **364**: 264–268.

[34] Donnelly NJ, Randall CA. Impedance spectroscopy of PZT ceramics-measuring diffusion coefficients, mixed conduction, and Pb loss. *IEEE Trans Ultrason, Ferroelect, Freq Contr* 2012, **59**: 1883–1887.

[35] Pandya S, Wilbur J, Kim J, *et al*. Pyroelectric energy conversion with large energy and power density in relaxor ferroelectric thin films. *Nat Mater* 2018, **17**: 432–438.

[36] Hardtl KH, Hennings D. Distribution of A-site and B-site vacancies in (Pb, La)(Ti, Zr)O_3 ceramics. *J Am Ceram Soc* 1972, **55**: 230–231.

[37] Zhu WL, Fujii I, Ren W, *et al*. Domain wall motion in A and B site donor-doped $Pb(Zr_{0.52}Ti_{0.48})O_3$ films. *J Am Ceram Soc* 2012, **95**: 2906–2913.

[38] Zhou H, Wu GH, Qin N, *et al*. Improved electrical properties and strong red emission of Pr^{3+}-doped $xK_{0.5}Bi_{0.5}TiO_3$–$(1–x)Na_{0.5}Bi_{0.5}TiO_3$ lead-free ferroelectric thin films. *J Am Ceram Soc* 2012, **95**: 483–486.

[39] Zhou H, Wu GH, Qin N, *et al*. Dual enhancement of photoluminescence and ferroelectric polarization in Pr^{3+}/La^{3+}-codoped bismuth titanate thin films. *J Am Ceram Soc* 2010, **93**: 2109–2112.

[40] Huang WH, He S, Hao AZ, *et al*. Structural phase transition, electrical and photoluminescent properties of Pr^{3+}-doped $(1-x)Na_{0.5}Bi_{0.5}TiO_3$–$xSrTiO_3$ lead-free ferroelectric thin films. *J Eur Ceram Soc* 2018, **38**: 2328–2334.

[41] Li LY, Castaing V, Rytz D, *et al*. Tunable trap depth for persistent luminescence by cationic substitution in Pr^{3+}:$K_{1-x}Na_xNbO_3$ perovskites. *J Am Ceram Soc* 2019, **102**: 2629– 2639.

[42] Bassiri-Gharb N, Fujii I, Hong E, *et al*. Domain wall contributions to the properties of piezoelectric thin films. *J Electroceram* 2007, **19**: 49–67.

[43] Keech R, Shetty S, Kuroda MA, *et al*. Lateral scaling of $Pb(Mg_{1/3}Nb_{2/3})O_3$–$PbTiO_3$ thin films for piezoelectric logic applications. *J Appl Phys* 2014, **115**: 234106.

[44] Kyômen T, Sakamoto R, Sakamoto N, *et al*.

Photoluminescence properties of Pr-doped (Ca, Sr, Ba)TiO_3. *Chem Mater* 2005, **17**: 3200–3204.

[45] Du XR, Huang WH, Thatikonda SK, *et al*. Improved ferroelectric and dielectric properties of Sm, La co-doped $Bi_4Ti_3O_{12}$ multifunctional thin films with orange-red emission. *J Mater Sci: Mater Electron* 2019, **30**: 13158–13166.

[46] Haertling GH. PLZT electrooptic materials and applications—A review. *Ferroelectrics* 1987, **75**: 25–55.

[47] Ma ZM, Zhang YC, Lu CJ, *et al*. Synthesis and properties of La-doped PMN–PT transparent ferroelectric ceramics. *J Mater Sci: Mater Electron* 2018, **29**: 6985–6990.

[48] Lin DB, Li ZR, Zhang SJ, *et al*. Electric-field and temperature induced phase transitions in $Pb(Mg_{1/3}Nb_{2/3})O_3$–$0.3PbTiO_3$ single crystals. *J Appl Phys* 2010, **108**: 034112.